SCIENCE CHINA
Chemistry

•ARTICLES•

April 2021 Vol.64 No.4: 608–615
https://doi.org/10.1007/s11426-020-9921-4

Improving current and mitigating energy loss in ternary organic photovoltaics enabled by two well-compatible small molecule acceptors

Yanna Sun[1†], Huan-Huan Gao[1†], Simin Wu[1†], Lingxian Meng[1], Xiangjian Wan[1], Mengyang Li[2], Zaifei Ma[2], Ziqi Guo[1], Shitong Li[1], Hongtao Zhang[1], Chenxi Li[1] & Yongsheng Chen[1*]

[1]*State Key Laboratory and Institute of Elemento-Organic Chemistry, The Centre of Nanoscale Science and Technology and Key Laboratory of Functional Polymer Materials, Institute of Polymer Chemistry, Renewable Energy Conversion and Storage Center, College of Chemistry, Nankai University, Tianjin 300071, China;*

[2]*Center for Advanced Low-dimension Materials, Stage Key Laboratory for Modification of Chemical Fibers and Polymer Materials, College of Materials Science and Engineering, Donghua University, Shanghai 201620, China*

Received October 24, 2020; accepted December 11, 2020; published online February 7, 2021

Ternary organic photovoltaic (OPV) strategy is an effective but facile approach to enhance the photovoltaic performance for single-junction devices. Herein, a series of ternary OPVs were fabricated by employing a wide bandgap donor (PBDB-TF) and two acceptor-donor-acceptor (A-D-A)-type nonfullerene small molecule acceptors (NF-SMAs, called F-2Cl and 3TT-OCIC). As the third component, the near-infrared SMA, 3TT-OCIC, has complementary absorption spectrum, narrow bandgap and well-compatible crystallization property to the host acceptor (F-2Cl) for efficient ternary OPVs. With these, the optimal ternary devices yield significantly enhanced power conversion efficiency of 15.23%, one of the very few examples with PCE higher than 15% other than Y6 systems. This is mainly attributed to the increased short-circuit current density of 24.92 mA cm^{-2} and dramatically decreased energy loss of 0.53 eV. This work presents a successful example for simultaneously improving current, minimizing energy loss and together with modifying the morphology of active layers in OPVs, which will contribute to the further construction of high performance ternary OPVs.

organic photovoltaics, ternary devices, small molecule acceptors, film morphology, energy loss

Citation: Sun Y, Gao HH, Wu S, Meng L, Wan X, Li M, Ma Z, Guo Z, Li S, Zhang H, Li C, Chen Y. Improving current and mitigating energy loss in ternary organic photovoltaics enabled by two well-compatible small molecule acceptors. *Sci China Chem*, 2021, 64: 608–615, https://doi.org/10.1007/s11426-020-9921-4

1 Introduction

Organic photovoltaics (OPVs) have attracted extensive attention owing to their unique features of solution processability, flexibility and semi-transparency [1–4]. In the past decade, with the development and innovation of nonfullerene small molecule acceptors (NF-SMAs), OPVs have been witnessed significant progress with power conversion efficiencies (PCEs) over 17% [5–11]. The active layer of a typical OPV device usually consists of an electron donor and an electron acceptor, which form bulk heterojunction (BHJ) structure with bi-continuous interpenetrating networks, facilitating the charge separation and transportation [1–3,7,9]. However, binary BHJ-OPVs still suffer from some drawbacks. For example, the absorption range of a common photovoltaic material is relatively narrow, the driving force for charge generation and non-radiative recombination often

†These authors contributed equally to this work.
*Corresponding author (email: yschen99@nankai.edu.cn)

lead to large energy loss (E_{loss}), and also the morphology of active layer remains to be further improved [12,13]. To settle these problems, an effective but facile strategy is to fabricate ternary OPV devices *via* introducing a third component into the host binary system.

For ternary devices, complementary absorption from visible to near-infrared (NIR) range could be realized *via* carefully matching photovoltaic materials with different absorption ranges [14–17]. Yet at the same time maintaining or improving the morphology of active layers is a major challenge. Therefore, the choice of the third component becomes especially important, which requires to satisfy these conditions simultaneously, including offering a complementary absorption spectrum, forming cascade-energy-level alignment, and together working with as a morphological modifier [14–19]. Recently, ternary OPV devices based on acceptor-donor-acceptor (A-D-A)-type NF-SMAs have made significant process owing to their finely modified molecular structures, diverse absorption spectral range, easily tuned energy levels and crystallization properties [20–27]. Notably, A-D-A-type NF-SMAs have similar A-D-A-backbone structures, consisting of three components: conjugated fused-ring core, ending group and side chains. The compatibility and crystallization properties of A-D-A-type SMAs could be finely tuned by modulating the above three components [1–3,7,9]. Thus, ternary OPVs employing two well-compatible A-D-A-type SMAs should be a promising approach to concurrently broaden spectral range for light harvesting and modulate film morphology for ameliorating exciton dissociation and improving charge carrier transport and collection, leading to excellent short-circuit current density (J_{SC}) and fill factor (FF) [28,29].

Another challenge in ternary OPVs is to maintain or improve the open-circuit voltage (V_{OC}), which is predominantly associated with the energy loss (E_{loss}, typically >0.6 eV) [30–35]. The E_{loss} is defined as $E_g - qV_{OC}$ (E_g can be estimated from intersection of the absorption and emission of materials with lower bandgap), including three parts as shown in Eq. (1) [36]:

$$\begin{aligned} E_{loss} &= E_g - E_{CT} + q\Delta V_{rad} + q\Delta V_{non\text{-}rad} \\ &= \Delta E_{CT} + q\Delta V_{rad} + q\Delta V_{non\text{-}rad} \end{aligned} \quad (1)$$

where E_{CT} represents charge-transfer (CT) state energy, ΔE_{CT} is calculated from the difference between energy of the first singlet excited state and CT state, which is required for exciton separation, but resulting in E_{loss}. Encouragingly, ΔE_{CT} results (<0.05 eV) of recent high-performance nonfullerene OPVs are opening novel perspectives for suppressing E_{loss} [37–39]. $q\Delta V_{rad}$ is related to radiative recombination, which is inevitable for all types of photovoltaic devices. The third part, $q\Delta V_{non\text{-}rad}$ is caused by non-radiative recombination, which is also the leading cause of large E_{loss} in OPVs. Recently, considerable efforts for mitigating E_{loss} have been devoted to molecule optimization. For example, Hou's group [5] designed a chlorinated SMAs BTP-4Cl by replacing the fluorine with chlorine atoms in Y6, leading to a reduced $q\Delta V_{non\text{-}rad}$ of 0.206 eV. Besides material optimization, device engineering optimization also plays important roles in mitigating E_{loss}. Regarding to this approach, ternary OPVs is an emerging strategy [24,40]. Benefiting from the easily tuned energy levels of A-D-A-type SMAs, designing ternary OPVs *via* introducing a SMA with narrow bandgap should be a promising and facile approach to reduce E_{loss} and further improving the photovoltaic performance.

In this work, a near-infrared NF-SMA named 3TT-OCIC, was employed as a third component into the host binary system (PBDB-TF:F-2Cl) for fabricating efficient ternary OPVs. Particularly, 3TT-OCIC offers complementary absorption spectrum, narrow bandgap and well-compatible crystallization property to match our recently reported high-performance A-D-A type SMA (F-2Cl) [12]. These characteristics would be favorable for light harvesting, cascade-energy-level alignment and film morphology modulating. With these, the obtained optimal ternary devices deliver a significantly increased PCE of 15.23%, one of the very few examples with PCE higher than 15% other than Y6 systems. This should be attributed to the enhanced J_{SC} of 24.92 mA cm^{-2}, well-maintained V_{OC} and FF of 0.844 V and 72.4%, respectively. Furthermore, E_{loss} of the optimal ternary devices (0.53 eV) is dramatically reduced from that of binary PBDB-TF:F-2Cl host system (0.78 eV), mainly ascribing to the reduction of both ΔE_{CT} and $q\Delta V_{non\text{-}rad}$. These results provide comprehensive understanding for the role of two well-compatible A-D-A type SMAs in improving the photovoltaic performance of ternary OPVs.

2 Results and discussion

The chemical structures of donor PBDB-TF, two A-D-A type SMAs F-2Cl and 3TT-OCIC are presented in Figure 1(a). It is noteworthy that F-2Cl and 3TT-OCIC have similar A-D-A-backbone molecular structures, which are composed of the chlorinated 2-(2,3-dihydro-3-oxo-1*H*-inden-1-ylidene) propanedinitrile (INCN2Cl) ending units and conjugated fused-ring cores. These rather similar acceptor materials have good miscible behavior and compatibility in solid film state. To evaluate this, atomic force microscopy (AFM) and contact angle characterization of F-2Cl neat film and F-2Cl:3TT-OCIC blend film were carried out (Figures S1, S2, and Table S1, Supporting Information online). After introducing 3TT-OCIC to F-2Cl neat film, no obvious over-aggregation or isolated domains was observed in the blend film, which is a morphological indication of a possible good compatibility. In addition, the F-2Cl neat film and F-2Cl:3TT-OCIC blend film exhibit very similar contact angles and surface tensions,

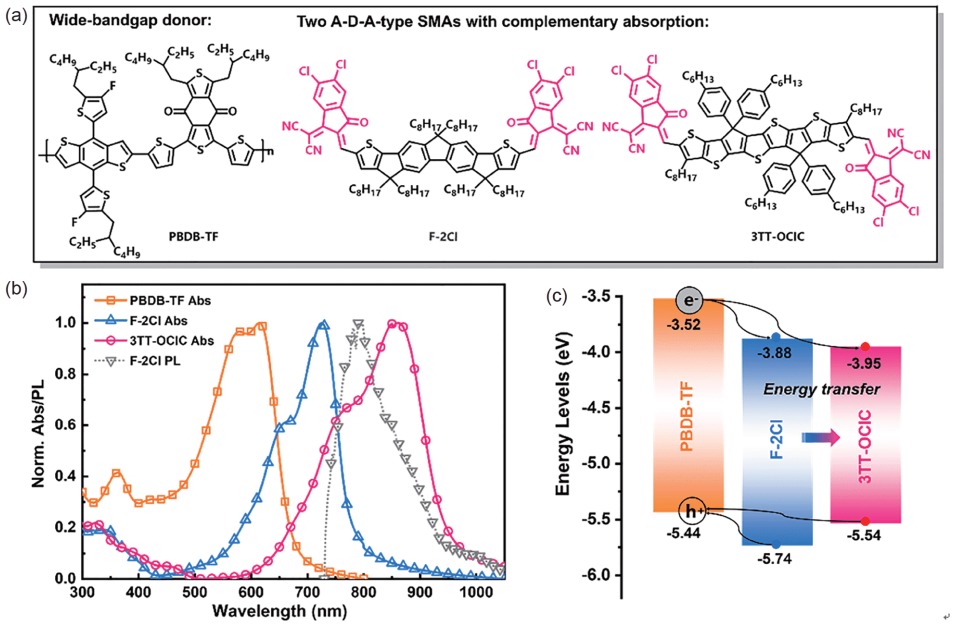

Figure 1 (a) Chemical structures of PBDB-TF, F-2Cl and 3TT-OCIC. (b) Normalized UV-Vis absorption spectra of PBDB-TF, F-2Cl and 3TT-OCIC neat films. Dot line shows the PL spectrum of F-2Cl films. (c) Energy levels diagram of PBDB-TF, F-2Cl and 3TT-OCIC (color online).

suggesting their well compatible property between the two acceptors [19,41]. As displayed in Figure 1(b), the ultraviolet-visible (UV-Vis) absorption spectra of PBDB-TF, F-2Cl and 3TT-OCIC in the film state present distinct absorption peaks at 615, 725, and 862 nm, respectively. Ternary components deliver complementary absorption spectrum covering from visible to NIR region, favorable for obtaining high J_{SC} in ternary OPVs. In addition, the energy level of three materials was measured by electrochemical cyclic voltammetry (CV) method (Figure S3). As shown in Figure 1(c), a cascaded lowest unoccupied molecular orbital (LUMO) level arrangement is formed among the three components, promoting the charge transport from donor to acceptors.

The photoluminescence (PL) spectrum was further measured to explore whether energy transfer existing between F-2Cl and 3TT-OCIC. As displayed in Figure 1(b), the PL of F-2Cl is fully covered by the absorption spectral of 3TT-OCIC, which is a clear indication of non-radiative energy transfer from F-2Cl to 3TT-OCIC [41,42]. To confirm this, PL spectra of F-2Cl and 3TT-OCIC neat film together with that of F-2Cl:3TT-OCIC blend were investigated with an excitation wavelength of 720 nm. As depicted in Figure 2(a), the F-2Cl:3TT-OCIC blend exhibits the same emission peak as 3TT-OCIC neat film at 958 nm. Interestingly, the PL emission of F-2Cl:3TT-OCIC blend film is significantly enhanced in the low energy region with intensity almost twofold higher than that of the neat 3TT-OCIC, while PL emission in the region of F-2Cl is fully diminished. These results powerfully demonstrated complete PL quenching of F-2Cl in the blend and efficient energy transfer from F-2Cl to 3TT-OCIC (Figure 1(c)). This can provide another possible channel for generating charges of F-2Cl excitons such as energy transfer to 3TT-OCIC and then hole to PBDB-TF [43,44]. These increased charge transfer channels can further improve the performance of ternary OPVs.

A series of OPV devices were fabricated with an inverted structure of indium tin oxide (ITO)/ZnO/PFN-Br/Active layer/MoO_3/Ag. After systematic device optimization (Tables S2–S5), a tiny amount of 1,8-diiodooctane (DIO, 0.3% volume) was added to the host solvent chloroform as solvent additive, and thermal annealing at 150 °C for 10 min was further performed for modifying morphology. The PBDB-TF:F-2Cl binary devices yielded a V_{OC} of 0.875 V, a J_{SC} of 19.97 mA cm^{-2} and an FF of 73.7%, delivering the maximum PCE of 12.87%. Besides, the PBDB-TF:3TT-OCIC binary devices exhibited a PCE of 12.43% with reduced V_{OC} (0.785 V) and FF (65.0%) but enhanced J_{SC} (24.40 mA cm^{-2}). The increased J_{SC} value is mainly ascribed to broad adsorption spectra to NIR region of 3TT-OCIC. To take advantages of its broaden absorption ability, different weight ratios of 3TT-OCIC were added into PBDB-TF:F-2Cl binary system as the third component for constructing ternary devices. The optimal ternary device was obtained with a composition of PBDB-TF:F-2Cl:3TT-OCIC=1:0.7:0.3 (Table 1). Compared with the host PBDB-TF:F-2Cl binary device, ternary device yielded an impressive PCE of 15.23%, one of the very few examples with PCE higher than 15% other than Y6 systems [9,14]. This should be attributed to the increased J_{SC} of 24.92 mA cm^{-2}, well-maintained V_{OC} and FF of 0.844 V and 72.4%, respectively. These results suggest that the ternary device reaches a relatively high V_{OC} with

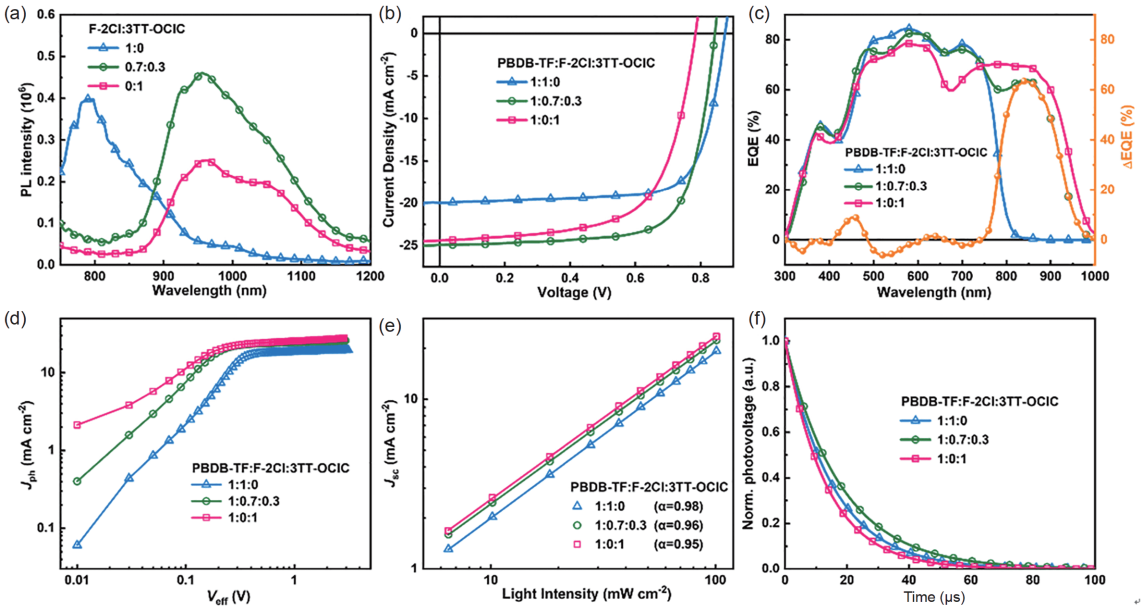

Figure 2 (a) PL spectra of F-2Cl, 3TT-OCIC neat films and F-2Cl:3TT-OCIC (0.7:0.3) blend film with the excitation wavelength of 720 nm. (b) *J-V* curves and (c) EQE spectra of the corresponding OPV devices, EQE offset (ΔEQE) between the optimal ternary devices and PBDB-TF:F-2Cl binary devices. (d) J_{ph} *versus* V_{eff} and (e) light-intensity dependence of J_{SC} and (f) transient photovoltage (TPV) of the optimal ternary and binary devices (color online).

Table 1 The photovoltaic parameters of binary and ternary OPV devices with different F-2Cl:3TT-OCIC weight ratios

PBDB-TF:F-2Cl:3TT-OCIC	V_{OC} (V)	J_{SC} (mA cm^{-2})	FF (%)	PCE_{max} (PCE_{ave}) [a] (%)
1:1:0	0.875 (0.872±0.003)	19.97 (19.63±0.25)	73.7 (72.7±0.6)	12.87 (12.56±0.27)
1:0.8:0.2	0.848 (0.843±0.004)	23.75 (23.45±0.20)	72.7 (71.8±0.4)	14.64 (14.32±0.19)
1:0.7:0.3	0.844 (0.839±0.004)	24.92 (24.56±0.14)	72.4 (71.6±0.6)	15.23 (15.01±0.26)
1:0.6:0.4	0.830 (0.827±0.003)	25.73 (25.35±0.23)	68.4 (67.2±0.6)	14.60 (14.43±0.31)
1:0.5:0.5	0.821 (0.818±0.003)	25.40 (25.20±0.17)	67.0 (66.1±0.5)	13.97 (13.72±0.23)
1:0:1	0.785 (0.783±0.003)	24.40 (24.21±0.15)	65.0 (64.3±0.3)	12.43 (12.11±0.28)

a) Average PCE values were calculated from 10 devices.

suppressed E_{loss}. Because the absorption edges of two SMAs in solid film state were different, the reduced E_{loss} for ternary OPVs may be ascribed to the reduction of ΔE_{CT} or $q\Delta V_{non\text{-}rad}$ as discussed below. The current density-voltage (*J-V*) curves of all devices were illustrated in Figure 2(b), and the detailed photovoltaic parameters are summarized in Table 1.

The external quantum efficiency (EQE) curves of binary and ternary devices were measured and shown in Figure 2(c). The PBDB-TF:F-2Cl devices exhibit relatively high EQE values of over 70% in the range from 470 to 750 nm, and PBDB-TF:3TT-OCIC devices show broad EQE range extending to 950 nm but with an apparent dip in the range of 640–730 nm. It is clearly observed that the two binary devices deliver well-complementary EQE spectra, indicating great potential for optimizing EQE response *via* ternary OPVs. As expected, with introducing 3TT-OCIC to PBDB-TF:F-2Cl host system, EQE response of ternary devices significantly enhanced and broadened. To visually presented the role of 3TT-OCIC addition in EQE spectra, EQE offset (ΔEQE) between the optimal ternary devices and PBDB-TF:F-2Cl host system was calculated as depicted in Figure 2(c). The positive ΔEQE values were observed in NIR region, and even with the highest value close to 70%, demonstrating the contribution of 3TT-OCIC (30 wt% in acceptors) to the dramatically enhanced J_{SC}. These observations were well consistent with the absorption variation trends of the corresponding blend films (Figure S4). These results reveal that ternary devices can provide good complementary absorption and efficiently improve the photoelectron conversion process. The integrated J_{SC} values of PBDB-TF:F-2Cl, PBDB-TF:F-2Cl:3TT-OCIC (1:0.7:0.3) and PBDB-TF:3TT-OCIC devices are calculated to be 18.69, 23.87 and 23.80 mA cm^{-2}, respectively, in agreement with the J_{SC} values obtained from the *J-V* curves.

The photoelectric physical process of the optimal binary and ternary devices was also studied and the curves of photocurrent (J_{ph}) *versus* effective applied voltage (V_{eff}) are presented in Figure 2(d). J_{ph} for the whole devices reach

saturation (J_{sat}) with V_{eff} value over 1.2 V, suggesting minimal charge recombination at high voltages [45]. Under the short circuit conditions, the ratio of J_{ph}/J_{sat} is 96% for ternary device, higher than those of PBDB-TF:F-2Cl and PBDB-TF:3TT-OCIC binary devices (94% and 91%), indicating enhanced exciton generation and charge collection efficiencies in ternary system. Besides, the α values of 0.98, 0.96 and 0.95 were observed from light-intensity (P) dependence of J_{SC} values for the PBDB-TF:F-2Cl, PBDB-TF:F-2Cl:3TT-OCIC and PBDB-TF:3TT-OCIC devices, respectively. These results suggest that the addition of 3TT-OCIC has a negligible effect on the bimolecular recombination of the host binary system [41]. Furthermore, charge transport properties in the corresponding films were investigated by the space-charge-limited current (SCLC) method (Figure S5). The electron and hole mobility for PBDB-TF:F-2Cl and PBDB-TF:3TT-OCIC binary devices are $4.16\times10^{-5}/3.61\times10^{-5}$ cm^2 V^{-1} s^{-1} (μ_e) and $2.85\times10^{-5}/5.08\times10^{-5}$ cm^2 V^{-1} s^{-1} (μ_h), respectively. Compared with the binary systems, the ternary device exhibits higher electron and hole mobility (μ_e=6.19×10^{-5} cm^2 V^{-1} s^{-1}, μ_h=1.18×10^{-4} cm^2 V^{-1} s^{-1}). In addition, as evidenced from transient photovoltage (TPV) (Figure 2(f)), the optimal ternary device demonstrates a longer carrier lifetime (17 μs) than those of PBDB-TF:F-2Cl and PBDB-TF:3TT-OCIC-based binary devices (15 and 13 μs). The enhanced charge transport and longer carrier lifetime for ternary devices contribute to suppressed charge recombination, supporting the enhanced J_{SC} and FF [46–48].

The morphological differences between the optimal binary and ternary blend films were characterized by AFM and transmission electron microscope (TEM) (Figure 3). In height images, PBDB-TF:F-2Cl blend exhibits smooth surface morphology and PBDB-TF:3TT-OCIC blend shows relative large aggregates with slightly larger root-mean-square (RMS) roughness of 2.82 nm. For the PBDB-TF:F-2Cl:3TT-OCIC ternary blend, clear nanofibrillar morphology with a smallest RMS of 1.65 nm was observed, which indicates that 3TT-OCIC is well-compatible with PBDB-TF:F-2Cl host blend, further obtaining fine morphology modification in ternary OPVs. Besides, in AFM and TEM images, the ternary blend displays obvious bicontinuous interpenetrating network with grain-like structures. The well-distributed morphology of ternary film is beneficial for exciton dissociation and charge transport, thus leading to higher J_{SC} [49,50].

To further explore the role of 3TT-OCIC in the morphology of active layer, grazing-incidence wide-angle X-ray scattering (GIWAXS) was performed to investigate the variations of molecular orientation. As depicted in Figure S6, F-2Cl pristine film exhibits (010) peak at 1.90 Å^{-1}, corresponding to a tight π-π stacking distance (d) of 3.31 Å, which indicates a preferential face-on molecular packing, while 3TT-OCIC shows a relatively weak π-π diffraction peak [51]. Apparently, both binary and ternary films display broad and

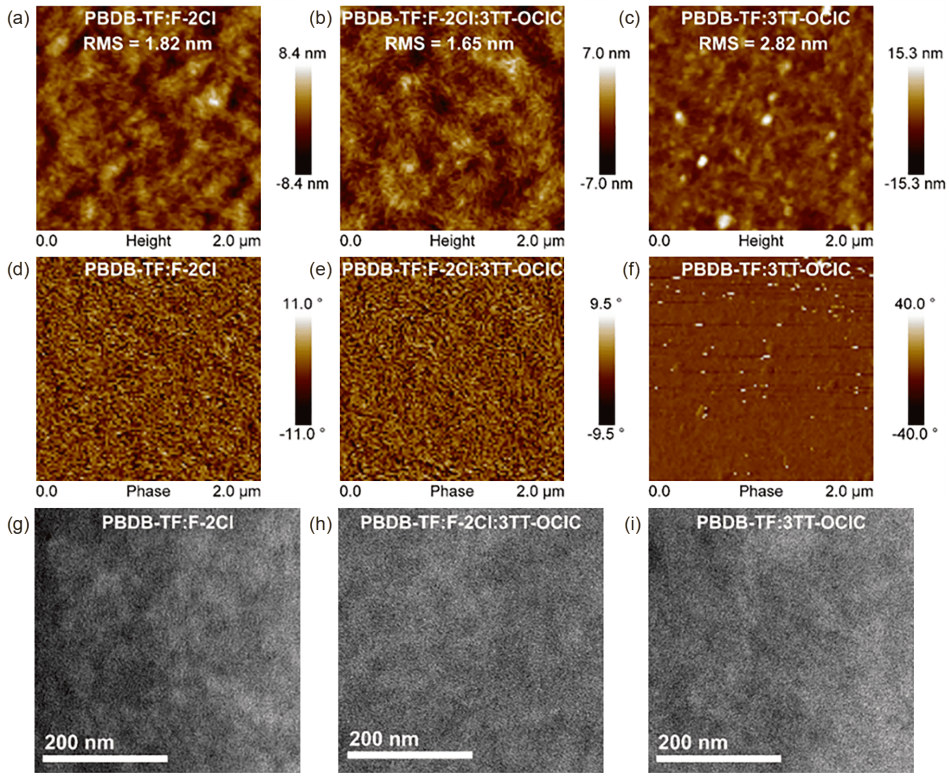

Figure 3 AFM height (upper), phase (middle) and TEM (lower) images for PBDB-TF:F-2Cl (a, d, g), PBDB-TF:F-2Cl:3TT-OCIC (1:0.7:0.3) (b, e, h) and PBDB-TF:3TT-OCIC (c, f, i) blend films (color online).

strong diffraction peak in the (010) regions (Figure 4), indicating a preferred face-on packing of PBDB-TF, F-2Cl and 3TT-OCIC in their corresponding blend films. For PBDB-TF:F-2Cl and PBDB-TF:3TT-OCIC binary blends, π-π stacking peaks located at 1.89 and 1.82 Å^{-1} (d=3.32 and 3.45 Å) can be observed. Interestingly, PBDB-TF:3TT-OCIC blend exhibits much greater crystal coherence length (CCL) (PBDB-TF:F-2Cl, 5.07 Å; PBDB-TF:3TT-OCIC, 18.85 Å) in the q_z direction, indicating enhanced crystallinity of PBDB-TF:3TT-OCIC blend film. Therefore, when a small amount 3TT-OCIC was added into PBDB-TF:F-2Cl binary system, the CCL significantly enhanced to 11.56 Å, suggesting an increase of the overall crystallinity for ternary blend film, favorable for charge transport. Altogether, the good-maintaining of face-on ordering and enhanced overall crystallinity with introducing of 3TT-OCIC should be responsible for the enhancement of photocurrent response in ternary OPVs.

In addition to significantly enhanced J_{SC} and improved film morphology, the effect of 3TT-OCIC on the well-maintained V_{OC} was further investigated. Detailed E_{loss} of optimized binary and ternary devices was thoroughly studied and presented in the Supporting Information online and Table 2. Based on the intersection of the absorption and emission of materials with lower bandgap, E_g, was estimated to be 1.65, 1.37 and 1.36 eV for the PBDB-TF:F-2Cl-, PBDB-TF:F-2Cl:3TT-OCIC- and PBDB-TF:3TT-OCIC-based devices, respectively (Figure S7). Thus, E_{loss} of 0.53 eV was achieved for the optimal ternary device, which is dramatically decreased from that of the binary PBDB-TF:F-2Cl host system (0.78 eV). E_{loss} of 0.53 eV is one of the lowest values reported for high-performance OPVs [14–16,24]. The suppressed E_{loss} by incorporating appropriate SMA 3TT-OCIC plays a vital role in the performance improvement of ternary OPVs.

To exactly confirm the contribution of three parts of E_{loss}, highly sensitive EQE (sEQE) and electroluminescence (EL) spectra of corresponding devices were measured. As displayed in Figure 5, E_{CT} was calculated from sEQE measurement with black body correction to be 1.48, 1.36, and

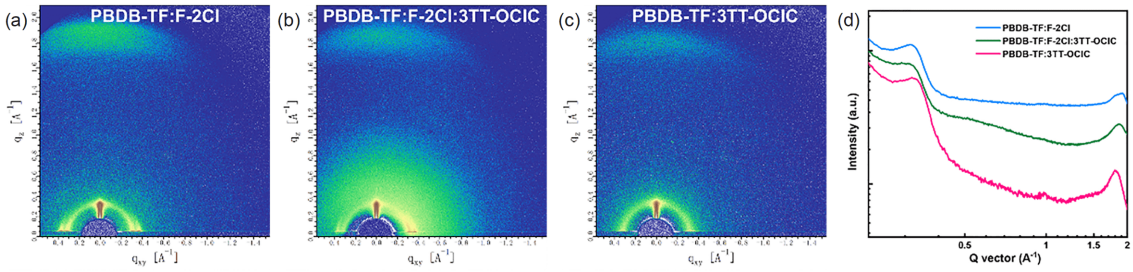

Figure 4 GIWAXS patterns of the PBDB-TF:F-2Cl (a), PBDB-TF:F-2Cl:3TT-OCIC (1:0.7:0.3) (b) and PBDB-TF:3TT-OCIC blend films (c). (d) Out-of-plane line cuts of the corresponding GIWAXS patterns (color online).

Table 2 Total and detailed E_{loss} of OPVs based on the binary and ternary devices

PBDB-TF:F-2Cl:3TT-OCIC	E_g (eV)	qV_{OC} (eV)	E_{loss} (eV)	E_{CT} (eV)	ΔE_{CT} (eV)	$q\Delta V_{rad}$ (eV)	$q\Delta V_{non\text{-}rad}$ (eV)	EQE_{EL}
1:1:0	1.65	0.875	0.78	1.48	0.17	0.28	0.33	1.53×10^{-6}
1:0.7:0.3	1.37	0.844	0.53	1.36	0.02	0.32	0.21	2.27×10^{-4}
1:0:1	1.36	0.785	0.58	1.32	0.04	0.33	0.21	2.16×10^{-4}

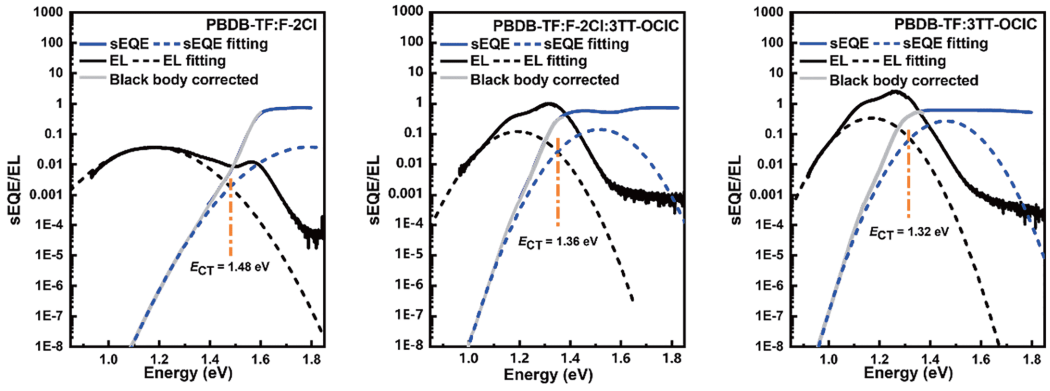

Figure 5 Reduced sEQE and EL spectra of the binary and ternary devices (color online).

1.32 eV for PBDB-TF:F-2Cl-, PBDB-TF:F-2Cl:3TT-OCIC- and PBDB-TF:3TT-OCIC-based devices, respectively [5]. Accordingly, ΔE_{CT} of 0.17, 0.02 and 0.04 eV for the above three devices were obtained, respectively. Notably, ΔE_{CT} of 0.02 eV for the ternary device was extremely low. The third part $\Delta V_{non\text{-}rad}$ is linearly related to the natural logarithm of electroluminescence quantum efficiency (EQE_{EL}). The optimal ternary devices yield higher EQE_{EL} of 2.27×10^{-4} than those of two binary devices (Table 2). Consequently, the calculated $\Delta V_{non\text{-}rad}$ of PBDB-TF:F-2Cl-, PBDB-TF:F-2Cl:3TT-OCIC- and PBDB-TF:3TT-OCIC-based devices were 0.33, 0.21 and 0.21 V respectively. These results clearly demonstrated that the well-maintained V_{OC} in ternary device is ascribed to the both reduction of ΔE_{CT} and $q\Delta V_{non\text{-}rad}$ with the addition of 3TT-OCIC.

3 Conclusions

In summary, efficient ternary OPVs with significant current enhancement of 25% and extremely low E_{loss} of 0.53 eV were successfully demonstrated *via* introducing an A-D-A type SMA (3TT-OCIC) to the binary PBDB-TF:F-2Cl host system. Therefore, the PCE increased dramatically from 12.87% and 12.43% of the binary devices to 15.23% for the optimal ternary OPVs, one of the very few examples with PCE higher than 15% other than Y6 systems. The third component 3TT-OCIC not only broaden the absorption spectrum range but also finely modify the film morphology in the ternary blends. Also efficient energy transfer was observed between the two acceptors. These factors should account for the significantly increased J_{SC} and well-maintained FF. Furthermore, reduction of both ΔE_{CT} and $q\Delta V_{non\text{-}rad}$ after introducing 3TT-OCIC should be the leading cause for the small E_{loss} of 0.53 eV and high V_{OC} of 0.844 V in ternary devices. These results suggest that combining two well-complementary and compatible A-D-A type SMAs for ternary OPVs could be an effective strategy to achieve simultaneously current improvement, E_{loss} suppression and morphology optimization. Thus, our designing strategy can offer good guidelines for further construction of highly efficient ternary OPVs.

Acknowledgements This work was supported by the National Key Research and Development Program of China (2019YFA0705900, 2016YFA0200200), the National Natural Science Foundation of China (21935007, 51873089, 51773095), Tianjin city (20JCZDJC00740, 17JCJQJC44500) and 111 Project (B12015).

Conflict of interest The authors declare no conflict of interest.

Supporting information The supporting information is available online at http://chem.scichina.com and http://link.springer.com/journal/11426. The supporting materials are published as submitted, without typesetting or editing. The responsibility for scientific accuracy and content remains entirely with the authors.

1 Qian D, Zheng Z, Yao H, Tress W, Hopper TR, Chen S, Li S, Liu J, Chen S, Zhang J, Liu XK, Gao B, Ouyang L, Jin Y, Pozina G, Buyanova IA, Chen WM, Inganäs O, Coropceanu V, Bredas JL, Yan H, Hou J, Zhang F, Bakulin AA, Gao F. *Nat Mater*, 2018, 17: 703–709
2 Yan C, Barlow S, Wang Z, Yan H, Jen AKY, Marder SR, Zhan X. *Nat Rev Mater*, 2018, 3: 18003
3 Zhang J, Tan HS, Guo X, Facchetti A, Yan H. *Nat Energy*, 2018, 3: 720–731
4 Sun Y, Chang M, Meng L, Wan X, Gao H, Zhang Y, Zhao K, Sun Z, Li C, Liu S, Wang H, Liang J, Chen Y. *Nat Electron*, 2019, 2: 513–520
5 Cui Y, Yao H, Zhang J, Zhang T, Wang Y, Hong L, Xian K, Xu B, Zhang S, Peng J, Wei Z, Gao F, Hou J. *Nat Commun*, 2019, 10: 2515
6 Kan B, Feng H, Yao H, Chang M, Wan X, Li C, Hou J, Chen Y. *Sci China Chem*, 2018, 61: 1307–1313
7 Liu S, Yuan J, Deng W, Luo M, Xie Y, Liang Q, Zou Y, He Z, Wu H, Cao Y. *Nat Photonics*, 2020, 14: 300–305
8 Meng L, Zhang Y, Wan X, Li C, Zhang X, Wang Y, Ke X, Xiao Z, Ding L, Xia R, Yip HL, Cao Y, Chen Y. *Science*, 2018, 361: 1094–1098
9 Wan X, Li C, Zhang M, Chen Y. *Chem Soc Rev*, 2020, 49: 2828–2842
10 Fei H. *Acta Polym Sin*, 2018, 9: 1141–1143
11 Nian L, Kan Y, Gao K, Zhang M, Li N, Zhou G, Jo SB, Shi X, Lin F, Rong Q, Liu F, Zhou G, Jen AKY. *Joule*, 2020, doi: 10.1016/j.joule.2020.1008.1011
12 Zhang Y, Feng H, Meng L, Wang Y, Chang M, Li S, Guo Z, Li C, Zheng N, Xie Z, Wan X, Chen Y. *Adv Energy Mater*, 2019, 9: 1902688
13 Sun Y, Gao HH, Yi YQQ, Wan X, Feng H, Ke X, Zhang Y, Yan J, Li C, Chen Y. *Sci China Mater*, 2019, 62: 1210–1217
14 Liu T, Luo Z, Chen Y, Yang T, Xiao Y, Zhang G, Ma R, Lu X, Zhan C, Zhang M, Yang C, Li Y, Yao J, Yan H. *Energy Environ Sci*, 2019, 12: 2529–2536
15 Ma X, Wang J, Gao J, Hu Z, Xu C, Zhang X, Zhang F. *Adv Energy Mater*, 2020, 10: 2001404
16 Zhan L, Li S, Zhang H, Gao F, Lau TK, Lu X, Sun D, Wang P, Shi M, Li CZ, Chen H. *Adv Sci*, 2018, 5: 1800755
17 Zhou Z, Xu S, Song J, Jin Y, Yue Q, Qian Y, Liu F, Zhang F, Zhu X. *Nat Energy*, 2018, 3: 952–959
18 Gao HH, Sun Y, Wan X, Ke X, Feng H, Kan B, Wang Y, Zhang Y, Li C, Chen Y. *Adv Sci*, 2018, 5: 1800307
19 Kan B, Yi YQQ, Wan X, Feng H, Ke X, Wang Y, Li C, Chen Y. *Adv Energy Mater*, 2018, 8: 1800424
20 Cui Y, Yao H, Zhang J, Xian K, Zhang T, Hong L, Wang Y, Xu Y, Ma K, An C, He C, Wei Z, Gao F, Hou J. *Adv Mater*, 2020, 32: 1908205
21 Lin Y, Adilbekova B, Firdaus Y, Yengel E, Faber H, Sajjad M, Zheng X, Yarali E, Seitkhan A, Bakr OM, El-Labban A, Schwingenschlögl U, Tung V, McCulloch I, Laquai F, Anthopoulos TD. *Adv Mater*, 2019, 31: 1902965
22 Liu Q, Jiang Y, Jin K, Qin J, Xu J, Li W, Xiong J, Liu J, Xiao Z, Sun K, Yang S, Zhang X, Ding L. *Sci Bull*, 2020, 65: 272–275
23 Yao J, Qiu B, Zhang ZG, Xue L, Wang R, Zhang C, Chen S, Zhou Q, Sun C, Yang C, Xiao M, Meng L, Li Y. *Nat Commun*, 2020, 11: 2726
24 Yu R, Yao H, Cui Y, Hong L, He C, Hou J. *Adv Mater*, 2019, 31: 1902302
25 Yuan J, Zhang Y, Zhou L, Zhang G, Yip HL, Lau TK, Lu X, Zhu C, Peng H, Johnson PA, Leclerc M, Cao Y, Ulanski J, Li Y, Zou Y. *Joule*, 2019, 3: 1140–1151
26 Zhan L, Li S, Lau TK, Cui Y, Lu X, Shi M, Li CZ, Li H, Hou J, Chen H. *Energy Environ Sci*, 2020, 13: 635–645
27 Luo Z, Ma R, Liu T, Yu J, Xiao Y, Sun R, Xie G, Yuan J, Chen Y, Chen K, Chai G, Sun H, Min J, Zhang J, Zou Y, Yang C, Lu X, Gao F, Yan H. *Joule*, 2020, 4: 1236–1247
28 Kumari T, Lee SM, Kang SH, Chen S, Yang C. *Energy Environ Sci*, 2017, 10: 258–265
29 Zhang J, Zhang Y, Fang J, Lu K, Wang Z, Ma W, Wei Z. *J Am Chem Soc*, 2015, 137: 8176–8183
30 Baran D, Kirchartz T, Wheeler S, Dimitrov S, Abdelsamie M, Gorman

J, Ashraf RS, Holliday S, Wadsworth A, Gasparini N, Kaienburg P, Yan H, Amassian A, Brabec CJ, Durrant JR, McCulloch I. *Energy Environ Sci*, 2016, 9: 3783–3793
31 Janssen RAJ, Nelson J. *Adv Mater*, 2013, 25: 1847–1858
32 Kranthiraja K, Kim S, Lee C, Gunasekar K, Sree VG, Gautam B, Gundogdu K, Jin SH, Kim BJ. *Adv Funct Mater*, 2017, 27: 1701256
33 Li Y, Lee DH, Lee J, Nguyen TL, Hwang S, Park MJ, Choi DH, Woo HY. *Adv Funct Mater*, 2017, 27: 1701942
34 Nguyen TL, Lee C, Kim H, Kim Y, Lee W, Oh JH, Kim BJ, Woo HY. *Macromolecules*, 2017, 50: 4415–4424
35 Wang C, Zhang W, Meng X, Bergqvist J, Liu X, Genene Z, Xu X, Yartsev A, Inganäs O, Ma W, Wang E, Fahlman M. *Adv Energy Mater*, 2017, 7: 1700390
36 Vandewal K, Benduhn J, Nikolis VC. *Sustain Energy Fuels*, 2018, 2: 538–544
37 Fu H, Wang Y, Meng D, Ma Z, Li Y, Gao F, Wang Z, Sun Y. *ACS Energy Lett*, 2018, 3: 2729–2735
38 Rosenthal KD, Hughes MP, Luginbuhl BR, Ran NA, Karki A, Ko S-J, Hu H, Wang M, Ade H, Nguyen T-Q. *Adv Energy Mater*, 2019, 9: 1901077
39 Zhong Y, Causa' M, Moore GJ, Krauspe P, Xiao B, Günther F, Kublitski J, Shivhare R, Benduhn J, BarOr E, Mukherjee S, Yallum KM, Réhault J, Mannsfeld SCB, Neher D, Richter LJ, DeLongchamp DM, Ortmann F, Vandewal K, Zhou E, Banerji N. *Nat Commun*, 2020, 11: 833
40 Ma X, An Q, Ibraikulov OA, Lévêque P, Heiser T, Leclerc N, Zhang X, Zhang F. *J Mater Chem A*, 2020, 8: 1265–1272
41 Yu R, Zhang S, Yao H, Guo B, Li S, Zhang H, Zhang M, Hou J. *Adv Mater*, 2017, 29: 1700437
42 An Q, Zhang F, Zhang J, Tang W, Deng Z, Hu B. *Energy Environ Sci*, 2016, 9: 281–322
43 Huang JS, Goh T, Li X, Sfeir MY, Bielinski EA, Tomasulo S, Lee ML, Hazari N, Taylor AD. *Nat Photon*, 2013, 7: 479–485
44 Zhang G, Zhang K, Yin Q, Jiang XF, Wang Z, Xin J, Ma W, Yan H, Huang F, Cao Y. *J Am Chem Soc*, 2017, 139: 2387–2395
45 Zhang ZG, Qi B, Jin Z, Chi D, Qi Z, Li Y, Wang J. *Energy Environ Sci*, 2014, 7: 1966–1973
46 Baumann A, Lorrmann J, Rauh D, Deibel C, Dyakonov V. *Adv Mater*, 2012, 24: 4381–4386
47 Maurano A, Hamilton R, Shuttle CG, Ballantyne AM, Nelson J, O'Regan B, Zhang W, McCulloch I, Azimi H, Morana M, Brabec CJ, Durrant JR. *Adv Mater*, 2010, 22: 4987–4992
48 Shuttle CG, O'Regan B, Ballantyne AM, Nelson J, Bradley DDC, Durrant JR. *Phys Rev B*, 2008, 78: 113201
49 Huang Y, Kramer EJ, Heeger AJ, Bazan GC. *Chem Rev*, 2014, 114: 7006–7043
50 Xia T, Cai Y, Fu H, Sun Y. *Sci China Chem*, 2019, 62: 662–668
51 Gao H-, Sun Y, Cai Y, Wan X, Meng L, Ke X, Li S, Zhang Y, Xia R, Zheng N, Xie Z, Li C, Zhang M, Yip H-L, Cao Y, Chen Y. *Adv Energy Mater*, 2019, 9: 1901024